

Effect of 2-Butyne-1, 4-Diol on the Nanostructure and Corrosion Resistance Properties of Electrodeposited Ni-W-B Coatings

M.G. Hosseini^{1,*}, M. Abdolmaleki¹, H. Ebrahimzadeh², S.A. Seyed Sadjadi²

¹ Electrochemistry Research Laboratory, Department of Physical Chemistry, Chemistry Faculty, University of Tabriz, Iran

² Department of Chemistry, IUST University, Tehran, Iran

*E-mail: mg-hosseini@tabrizu.ac.ir

Received: 24 October 2010 / Accepted: 20 January 2011 / Published: 1 April 2011

The paper reports a study on the influence of 2-butyne-1, 4-diol brightener on the electrochemical corrosion behavior of electrodeposited nanocrystalline Ni-W-B alloy coatings. Corrosion behavior of the coatings deposited on copper substrates was studied at different immersion times in 3.5% NaCl solution by using electrochemical impedance spectroscopy while their passivation behavior was studied in 1N sulphuric acid solution by using potentiodynamic polarization. Scanning electron microscopy and X-ray diffraction were used to characterize the morphology and surface analysis, respectively. A full-bright and smooth Ni-W-B alloy can be electrodeposited in the presence of 2-butyne-1, 4-diol. It is found that appropriate amount of this additive could lead to finer structure and higher hardness of the deposit. The electrochemical impedance spectroscopy results exhibited that the higher corrosion resistance of the nanocrystalline Ni-W-B electrodeposited from solution containing 2-butyne-1, 4-diol is due to the preferential dissolution of nickel and formation of a tungsten rich film on the surface. Potentiodynamic polarization studies exhibited that regardless of composition, all the alloys exhibited passivation behavior over a wide range of anodic potentials. The impedance data for optimum coating represented different behavior at applied anodic potential in 1N sulphuric acid solution.

Keywords: Nanostructures, coatings, corrosion test, hardness

1. INTRODUCTION

The electroplating of steel sheets and tubes used in many applications include plating by copper, nickel and chromium. Decorative chromium coatings are applied from hexavalent chromium processes based on chromic acid. Hexavalent chromium in solution is a recognized carcinogen and causes other health problems such as skin and lung irritation [1, 3]. Due to these reasons, replacement of chrome coatings by another process has been required. Electrodeposition of alloys is particularly

important for applications in microfabrication technologies. The electrodeposition of pure tungsten coatings from tungstate solutions is hindered by the formation of an oxide layer on the cathode during electrodeposition. This oxide cannot be directly reduced to metallic tungsten because of the very low overvoltage for hydrogen evolution on tungsten. Hence, a further reduction to metallic tungsten does not proceed, and the entire current is consumed for hydrogen evolution [4, 5]. Tungsten and molybdenum ions do co-deposit with iron group metals so that alloys containing a high content of refractory elements are obtained [6-9]. This phenomenon is called induced co-deposition [9]. Electrodeposited tungsten alloys possess attractive corrosion and tribological properties [8-13]. Therefore such coatings were considered recently as an alternative to electrolytic chromium coatings. The electrochemical synthesis of W and Mo based alloys has essential advantages compared to the electrodeposition of chromium in terms of ecological and health risks [14-16]. It is well known that good appearance is very important for application of a new electroplating technology, but few papers studied the brightness of deposited Ni-W-B alloy, one reason may be those Na_2WO_4 and complexing agents which are often used have positive effect on the appearance of Ni-W-B deposit. Generally, Ni-W alloys are known to exhibit higher hardness, higher heat resistance and also a better corrosion behavior compared to elemental Ni [17]. During the corrosion process tungsten preferentially migrated toward the surface and formed oxides. In our previous study, for the first time, optimized Ni-W-B alloys were prepared from tartrate bath [18-20]. Some of the advantages of tartrate baths as compared to ammonia citrate baths are electroplating in the acidic medium, higher current efficiency and increase of tungsten content in the deposit that leads to the formation of nanocrystalline or amorphous coatings with higher hardness and corrosion resistance. 2-butyne-1, 4-diol (BD) is used as corrosion inhibitor for mild steel, and Aluminum [21-22]. In this paper, we have studied the changes in morphology, composition and structure of the electrodeposited Ni-W-B coatings deposited from the optimum bath with different concentration of additive from tartrate bath. In addition, the influence of 2-butyne-1, 4-diol brightener (BD) on the corrosion resistance of electrodeposited Ni-W-B coatings was discussed through the application of electrochemical impedance spectroscopy (EIS) and potentiodynamic polarization.

2. EXPERIMENTAL

2.1. Sample preparation

Electrolyte was prepared by dissolving chemical reagents in triply distilled water. Nickel sulfate (Merck, 99% pure) and sodium tungstate (Merck, 99% pure) were incorporated in the bath as source of nickel and tungsten, respectively. Sodium borate (Merck, 99% pure) was added to the bath to provide a source of boron for creating hard deposit. Sodium potassium tartrate (Merck, 99% pure) and 2-butyne-1, 4-diol (Merck, 99% pure) were added as complexing agent for stability of the bath and brightener, respectively. The detailed chemical composition of electrolyte was listed in Table 1. The concentration of BD was varied from 0 to 1.5 g L^{-1} . All electrodeposition experiments were carried out at $60 \text{ }^\circ\text{C}$. A platinum sheet (geometric area 20cm^2) was used as an insoluble anode and copper sheets (geometric area 1 cm^2) were used as cathode. Before the electrodeposition, the cathode substrates were

polished mechanically to mirror finish with 2500 grit SiC paper, degreased in a 30% NaOH solution for 5 min, washed with distilled water, and dried in air. All specimens were etched in a 10% sulfuric acid solution for 2 min and then rinsed with deionized water and acetone then weighed prior to the plating process by a Mettler analytical balance with sensitivity of 0.01 mg.

Table 1. Composition and operating conditions of the Ni-W-B alloy plating bath

Chemical reagents	Concentration
NiSO ₄ ·6H ₂ O	0.076 mol L ⁻¹
NaKC ₄ O ₆ H ₄	0.404 mol L ⁻¹
Na ₂ WO ₄ ·2H ₂ O	0.197 mol L ⁻¹
Na ₂ B ₄ O ₇ ·10H ₂ O	0.13 mol L ⁻¹
2-butyne-1, 4-diol	Variable (0-1.5 g L ⁻¹)
Current density	40 mA cm ⁻²
Temperature	60 °C
pH	6.0

Deposition faradaic efficiency (FE) of the alloy was measured by using the following equation [23]:

$$FE = \frac{W}{It} \sum \frac{c_i n_i F}{BM_i} \times 100 \quad (1)$$

where W is the measured weight of the deposit (g), I is the current passed (A), t is the deposition time (h), C_i is the weight fraction of the element (nickel, tungsten and born) in the ternary alloy deposit, n_i is the number of electrons transferred in the reduction of 1 mol atoms of that element ($n_i = 2$ for nickel, 6 for tungsten and 3 for boron), M_i is the atomic weight of that element (g mol⁻¹), F is the Faraday constant (96,485.3Cmol⁻¹) and B is a unit conversion factor (3600 CA⁻¹h⁻¹). The partial currents of elements were also calculated using the deposit composition (w), the deposition time (t), the mass of the deposit (m) and electrochemical equivalent (e):

$$i_p = \frac{mw}{100et} \quad (2)$$

The hydrogen partial current density was determined by subtracting the sum of the metal current densities from the total applied current density.

2.2. Characterization

After electrodeposition, the sample was dissolved in an aqueous solution containing 250 g L^{-1} of CrO_3 and $15 \text{ cm}^3 \text{ L}^{-1}$ of H_2SO_4 by heating in 373 K and then the metal content was determined using a Varian inductively coupled plasma (ICP) instrument (model VARIAN/VISTA-PRO). The surface morphology of the Ni-W-B electrodeposits was characterized with a scanning electron microscope (SEM, Philips XL30 with EDAX DETECTING UNIT model NLW XL30 144-2.5). The thickness of the deposits was large enough (average thickness of $20 \mu\text{m}$) so that no signal from the underlying gold substrate was observed. Each sample was measured at different locations to confirm uniformity. The structure of deposits was studied using an X-ray diffraction (XRD) with Cu-K_α radiation (Philips PW-3020 Goniometer) operated at 40 kV and 200 mA. Microhardness of the deposits was determined by using a Vickers diamond pyramid model BUEHLER with a load of 10 g and loading time of 15 s. Each value was the average of five readings.

2.3. Electrochemical corrosion testing

Electrochemical impedance spectroscopy (EIS) and electrochemical potentiodynamic measurements were performed in a three-electrode cell arrangement. A platinum mesh of the geometric area of about 20 cm^2 was used as counter electrode, while all potentials were measured with respect to a commercial saturated calomel electrode (SCE). Electrochemical experiments were carried out using a Princeton Applied Research, EG&G PARSTAT 2263 Advanced Electrochemical system run by PowerSuite software. The r.m.s amplitude of the modulation potential for the EIS measurements was 10 mV, and the frequency range was from 100 kHz to 1 mHz. The acquired data were curve fitted and analyzed using ZView (II) software. Prior to potentiodynamic polarization measurements the samples were immersed in 1 N sulfuric acid solution for about 30 min in order to establish the open circuit potential (E_{OCP}). Potentiodynamic curves were recorded at a scan rate of 1 mV s^{-1} in the potential range of -0.1 V vs. open circuit potential to $+2.0 \text{ V}$ vs. SCE. In this work, the impedance spectra were recorded after different immersion times (30 min, 2 h, 4 h, 8 h, 12 h and 24 h) in 3.5% NaCl solution in order to compare corrosion resistance of Ni-W-B coatings deposited in solution with 0.5 g L^{-1} BD and without BD, then the influence of the different anodic potentials on the impedance pattern were studied for optimum coating in 1N sulphuric acid solution after potentiodynamic polarization measurements.

3. RESULTS AND DISCUSSIONS

3.1. Relationship between BD concentration and current efficiency

BD concentration in the electrolyte was found to be a direct factor influencing the composition of electrodeposited coatings. Figure 1 shows the effect of the concentration of BD on partial current density of W, H_2 and cathodic efficiency.

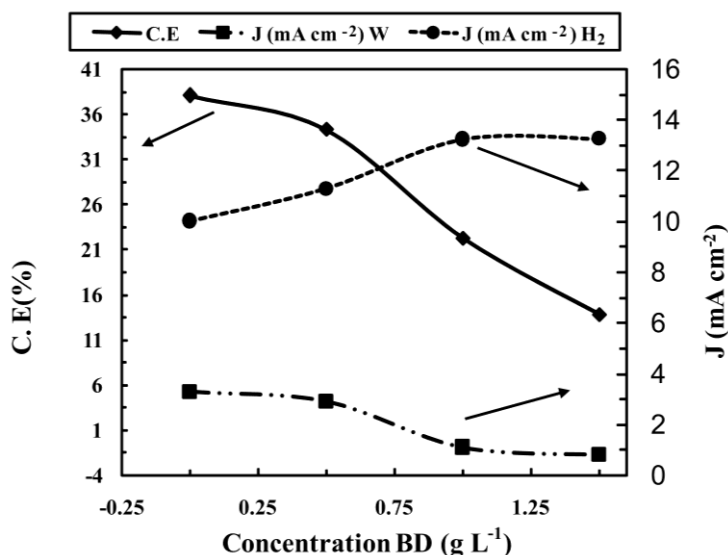


Figure 1. Effects of the concentrations of BD on partial current density of W, H₂ and cathodic efficiency.

As it can be seen from Figure 1, addition of BD decreases both W content in the deposit and the cathodic efficiency to a great extent. The results indicate that BD has more profound effects on hydrogen evolution reactions (HER, which is decided factor for the cathodic efficiency). It is thus reasonable to say that, during Ni-W-B plating, increasing BD concentration can accelerate HER and thereby decreases faradic deposition efficiency. One of the possible reasons behind decreasing the current efficiency is adsorption of BD on the plating surface decreasing the effective area on the electrode free for Ni-W-B electrodeposition. From Figure 1, it can be seen that the optimum concentration of BD is 0.5 g L⁻¹, because smooth and bright deposits, high W content as well as, current efficiency could be obtained from the electroplating bath. By using ICP analysis, the composition of alloys prepared from electrolyte with BD concentration of 0.5 g L⁻¹ and without it contains 38.94 wt. % and 44.12 wt. % tungsten, respectively.

3.2. Effects of BD on morphology and grain size of Ni-W-B alloy

Figure 2 shows the change in the surface morphology of the electrodeposited Ni-W-B alloy as a function of concentration of BD in solution.

The surface of Ni-44.12 wt. %W-1.86 wt. %B alloy electrodeposited from the plating bath without BD shows coarse nodular structure as the small globules superimposed on the bigger ones show that the surface is not uniform and composed of different sized domains (Figure 2(a)). A surface smoothing effect was observed with the addition of 0.5 g L⁻¹ BD to the bath solution (Figure 2(b)). The more smooth deposit is the Ni-34.83 wt. %W-1.86 wt. %B alloy prepared from electrolyte with BD concentration of 1 g L⁻¹ (Figure 2(c)). By increasing BD concentration beyond this value, the deposit appearance became slightly rougher and there were more micro-cracks at the deposits (Figure 2(d)). Generally, the brightener introduction has played a major role in reducing/inhibiting the activation of

additional nodule sites. This has led to refinement in microstructure and disappearance of nodules in the deposit. This could be the reason for obtaining very smooth and bright ternary Ni-W-B coating.

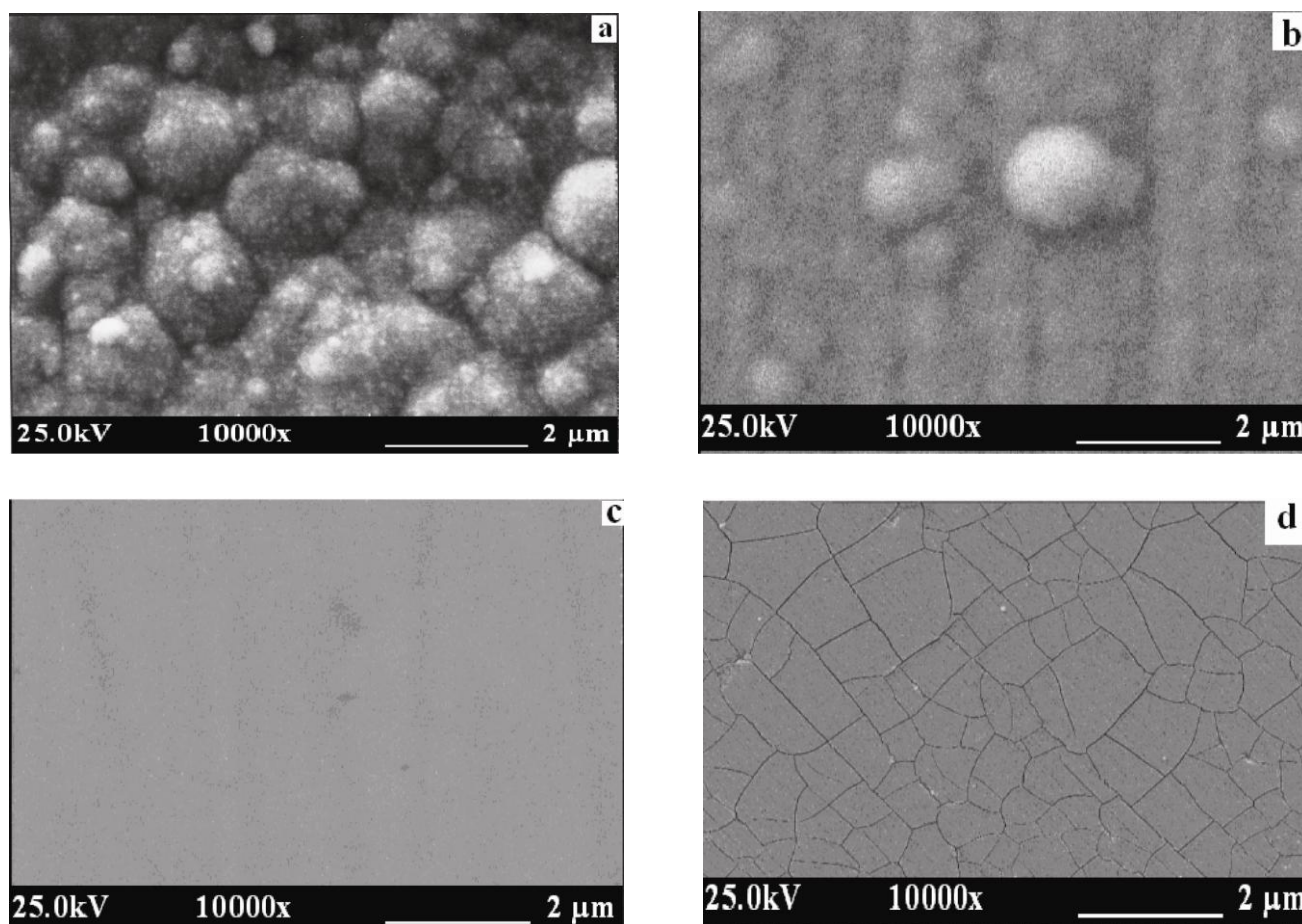


Figure 2. Surface morphology depending on BD concentration in electrolyte: (a) 0, (b) 0.5, (c) 1 and (d) 1.5 g L⁻¹.

3.3. XRD analysis of the deposits

The X-ray diffraction patterns of the Ni-W-B coatings deposited in solution with 0.5 g L⁻¹ BD and without it were shown in Figure 3, while corresponding peak positions and grain sizes are given in Table 2.

In all of diffraction patterns, the reflections corresponding to the (1 1 1) plane of a face centered cubic (fcc) phase of nickel can be observed and also it can be seen that the electrodeposited Ni-38.94 wt. %W-1.86 wt. %B coating with 0.5 g L⁻¹ concentration of BD has a crystallite size of 6 nm. The grain size was estimated using the (1 1 1) diffraction peak by applying the Scherrer equation [24]. A marginal increase in crystallite size (14 nm) has been observed for electrodeposited Ni-44.12 wt. %W-1.86 wt. %B coating from a solution without BD. A reduction in the peak width is also observed for electrodeposited Ni-W-B coating without BD compared to that obtained with BD in

solution. It was explained that as-deposited Ni-W-B alloys are supersaturated solid solutions of W and B in fcc nickel.

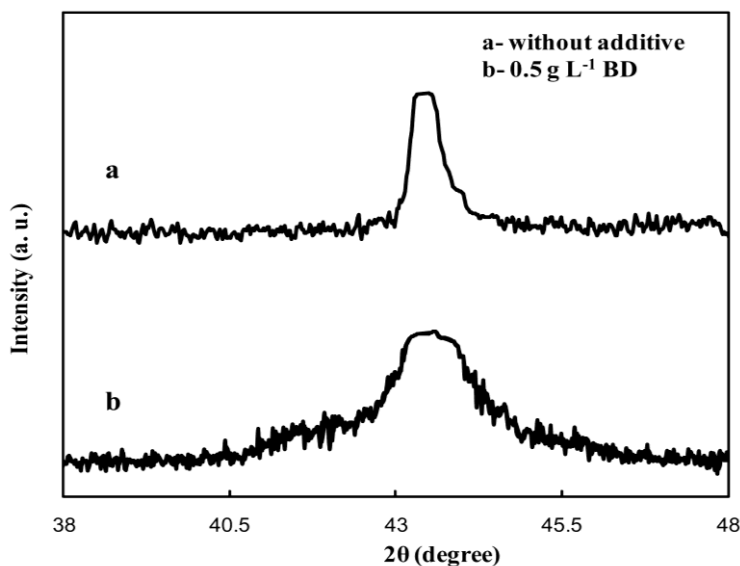


Figure 3. XRD patterns of Ni-W-B coatings deposited from the bath with and without additive.

Table 2. Peak position (2θ) and grain size (from Debye-Scherrer formula) for as-plated Ni-W-B coatings with and without BD in solution

Type of coating	Peak position	Grain size (nm)
as- plated Ni-W-B with BD	43.53	6
as- plated Ni-W-B without BD	43.31	14

Generally, the amorphous alloy structure must arise either because the deposition process produces mutually incoherent particles which are too small for the crystalline configuration to be formed energetically [25] or because the atoms do not bond together in the arrangement required for crystals long-range order [26].

3.4. Microhardness of the deposits

Figure 4 illustrates the relationships between microhardness and W content of Ni-W-B deposits with BD concentration in the electrolyte. As BD concentration was increased the W content decreased so that the deposit hardness increased from HV 825 to approximately HV 875 firstly as W content decreased from approximately 44 wt.% to approximately 39 wt.%, and then decreased to approximately HV 600 as tungsten content was approximately 32.5 wt.%. This would also be consistent with Figure 1.

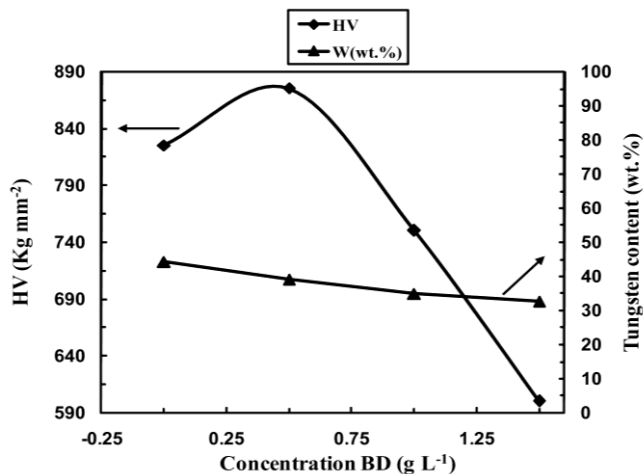


Figure 4. Effect of BD concentration in the electrolyte on the tungsten content and deposit microhardness

The hardness variation is believed to result from the grain size refinement effect of the addition of BD or sodium tungstate to the electrolyte. The maximum hardness was achieved for the Ni-38.94 wt. %W-1.86 wt. %B alloy, which was about 875 HV, as shown in Figure 4.

3.5. Electrochemical impedance spectroscopy studies

The equivalent circuit, Nyquist and Bode plots for Ni-W-B alloys plated at solutions with concentration of 0.5 g L⁻¹ BD and without it at different immersion times in 3.5% NaCl solution are shown in Figures 5, 6.

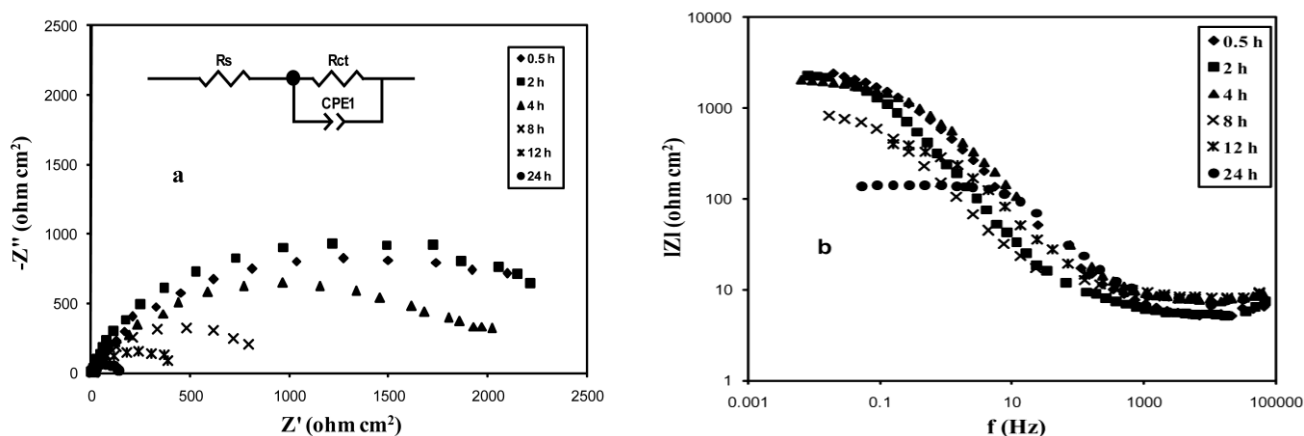


Figure 5. Equivalent circuit, Nyquist (a) and Bode plots (b) for Ni-44.12 wt. %W-1.86 wt. %B alloy deposited from solution without BD concentration after different immersion times.

In these Figures, almost all of the curves appear to be similar (Nyquist plots), consisting of a single semicircle in the investigated frequency region signifying the electron transfer reaction at the metal/solution interface. However, it should be noted that though these curves appear to be similar

with respect to their shape, they differ considerably in their size. This indicates that the same fundamental processes must be occurring on all these coatings but to different extent in each case. The dissolution of Ni species is due to the Cl^- attack (e.g. $\text{NiO} + \text{H}_2\text{O} \rightarrow \text{Ni}^{2+} + 2\text{OH}^-$). In addition, the formation of nickel oxide species (e.g. $\text{Ni}^{2+} + 2\text{H}_2\text{O} \rightarrow \text{Ni}(\text{OH})_2 + 2\text{H}^+$) should also provide the impedance at the electrolyte/hydroxide interface.

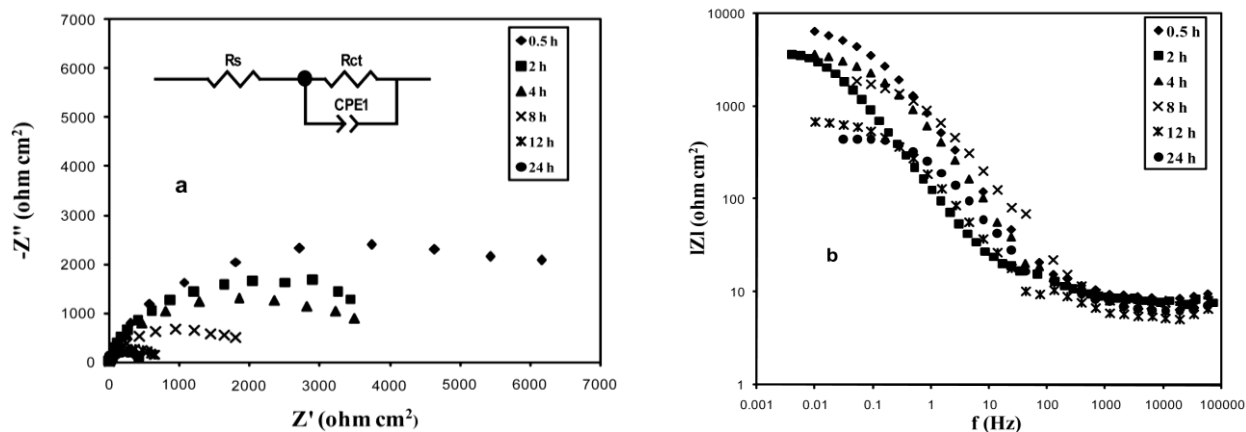


Figure 6. Equivalent circuit, Nyquist (a) and Bode plots (b) for Ni-38.94 wt. %W-1.86 wt. %B alloy deposited from solution with 0.5 g L^{-1} BD concentration after different immersion times.

Therefore, the above reactions can be modeled as a double-layer capacitor in parallel with a charge-transfer resistor.

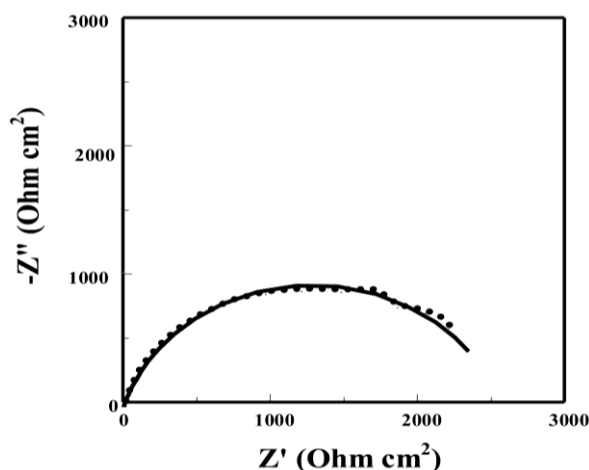


Figure 7. Nyquist diagram of impedance spectrum of experimental data (dots points) and fitting curve (solid line) for Ni-44.12 wt. %W-1.86 wt. %B alloy deposited from solution without BD concentration in 3.5 wt. % NaCl solution after 2 h of immersion.

The best equivalent circuit for the EIS spectra of the alloys is a randles-like model, designated as R_s - R_{ct} -CPE, in which the polarization charge transfer resistance (R_{ct}) is in parallel with a constant

phase element (CPE), and both of these elements are in series with the ohmic resistance (R_s), as shown in Figures 5, 6. In this model, constant- phase element may have some combination of capacitive, resistive and inductive character [27]. In this model, R_s is the total ohmic resistance of the electrochemical cell and contains contributions from the solution, cables and other sources.

R_{ct} is considered to be the corrosion resistance of the alloy, which is inversely proportional to the corrosion current density. The CPE is defined by two parameters, T and P, in the equation for impedance [28, 29].

$$Z = \frac{1}{T(j\omega)^p} \quad (3)$$

The value of the exponent P may vary from 0 to 1. If p equals 0, then the CPE is a resistor. A CPE is often used in an equivalent circuit model in place of a capacitor to compensate for inhomogeneity in the system. In Figure 7 is represented one experimental diagram together with the best fit curve in terms of equivalent circuit of Figures 5, 6. It could be observed that the experimental impedance data fit very well with the equivalent circuit proposed.

Table 3. Corrosion data obtained from EIS spectra in 3.5 wt. % NaCl solution after different immersion time calculated with equivalent circuit from figures 5 and 6.

Sample	Element	0.5 h	2 h	4 h	8 h	12 h	24 h
Without BD	R_s ($\Omega \text{ cm}^2$)	5.342	5.955	7.72	8.76	8.348	7.662
	CPE-T (F cm^{-2})	0.00046343	0.00090055	0.00033863	0.0017445	0.00061129	0.0001742
	CPE-P	0.750	0.798	0.764	0.761	0.77	0.811
	R_{ct} ($\Omega \text{ cm}^2$)	2832	2544	1979	963	450.6	137.6
	Error (%)	1.62	2.48	1.02	1.69	0.88	0.79
0.5 g L ⁻¹ BD	R_s ($\Omega \text{ cm}^2$)	8.989	9.119	8.321	7.094	5.803	6.681
	CPE-T (F cm^{-2})	0.0002959	0.0017028	0.00039721	0.00019877	0.0013926	0.00083553
	CPE-P	0.845	0.789	0.840	0.821	0.763	0.752
	R_{ct} ($\Omega \text{ cm}^2$)	6547	4733	3572	1859	725.1	488.9
	Error (%)	0.84	5.98	1.21	0.88	2.56	1.81

The best fit values of the equivalent-circuit elements for Ni-W-B alloys deposited at solutions with concentration of 0.5 g L⁻¹ BD and without it are listed in Table 3. The data in this Table indicate that the mean error of modulus is smaller than 6%, indicating a good fitting of the experimental data. In Table 3, the values of CPE-P for Ni-W-B alloys deposited at solutions with concentration of 0.5 g L⁻¹ BD are larger than those of the Ni-W-B alloys deposited at solutions without BD, indicating the smooth nature of these deposits.

The charge transfer resistance for Ni-W-B alloys as a function of the immersion time in 3.5 wt. % NaCl solution is shown in Figure 8.

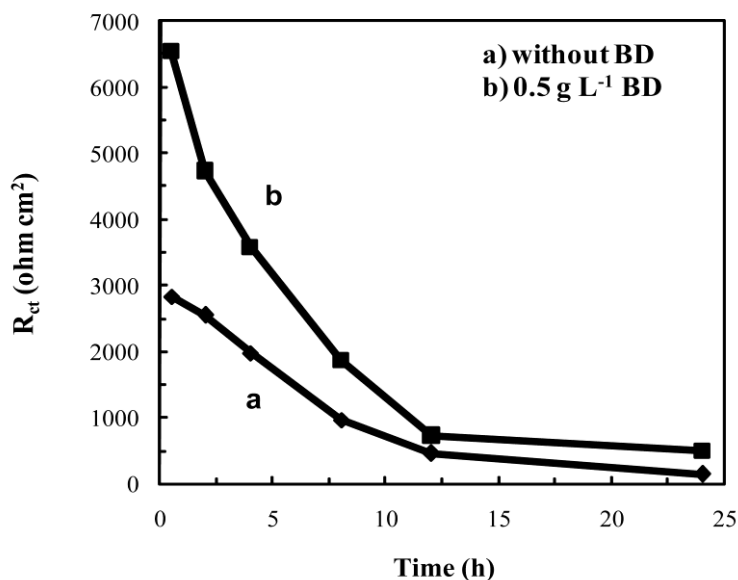


Figure 8. Calculated charge transfer resistance for Ni-W-B alloy coatings as a function of the immersion time in 3.5 wt. % NaCl solution

It can be seen that the charge transfer resistance of coatings decreased with increasing immersion time in 3.5 wt. % NaCl solution. Based on the results obtained from the impedance diagram the following conclusions can be drawn: The highest value of charge transfer resistance (6547 Ohm cm²) was obtained for Ni-W-B alloy deposited from solution with concentration of 0.5 g L⁻¹ BD after 0.5h immersion time.

The charge transfer resistance values of Ni-W-B alloys deposited at solutions with BD were higher compared to those of the alloys without BD, maybe it is due to the change in alloy electrodeposition mechanism and a decreases in the grain size as well as a total increase in the amorphousity of the alloy were evident as confirmed by XRD results shown in Figure 3. The Bode plots for all coatings showed similar trends and thus it can be concluded that only one mechanism prevailed for the corrosion of the coatings.

3.6. Potentiodynamic polarization studies

Potentiodynamic polarization curves were recorded for nanocrystalline Ni-38.94 wt. %W-1.86 wt. %B alloy, Ni-30.74 wt. %W-1.86 wt. %B alloy deposited from solution with 0.5 g L⁻¹ BD concentration in current density of 30 mA cm⁻² and conventional coarse-grained polycrystalline Ni-44.12 wt. %W-1.86 wt. %B alloy in 1 N H₂SO₄ solution (Figure 9).

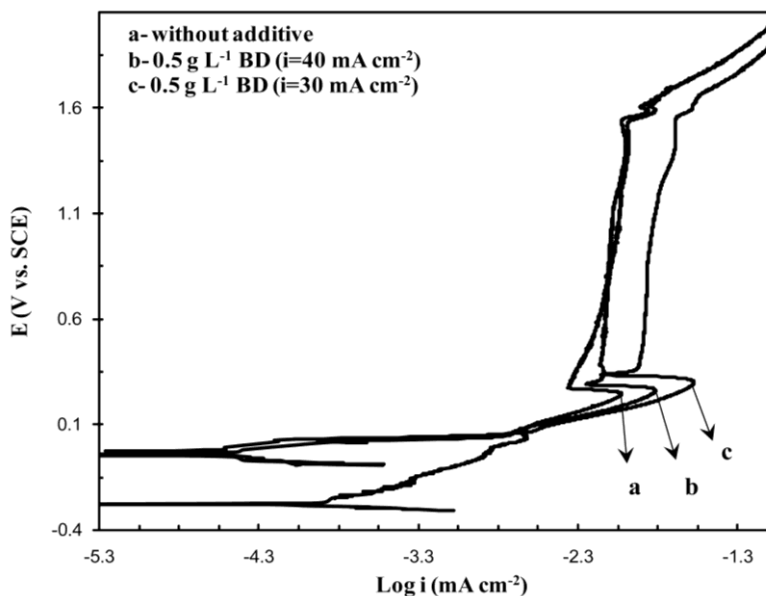
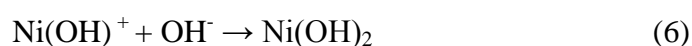
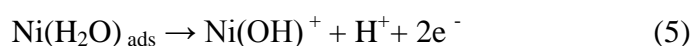


Figure 9. Potentiodynamic polarization curves of Ni-W-B coatings deposited from the bath with and without additive in 1 N H₂SO₄ at scan rate of 1 mV s⁻¹

Comparison of curves a-c, reveals two features; first, the sequence of deposits with respect to a less negative E_{ocp} is: Ni-44.12 wt. %W-1.86 wt. %B alloy (-0.28 V) << Ni-30.74 wt. %W-1.86 wt. %B alloy (-0.047 V) < Ni-38.94 wt. %W-1.86 wt. %B alloy (-0.027 V). This positive shift in E_{ocp} indicates the good anticorrosion property of nanocrystalline Ni-W-B coatings deposited in solution with 0.5 g L⁻¹ BD in sulfuric acid medium. The hydrogen evolution is the predominant reduction reaction in the present case. It is known that defects like dislocation, affects the kinetics of hydrogen evolution reaction. Moreover, reversible trapping of hydrogen at the dislocations, grain boundaries and voids (pores) can change the kinetics of hydrogen evolution. Second, the critical current densities of passivation for all the Ni-W-B samples were approximately similar. This indicates that the mechanism of onset of passivity and passivation itself is similar in nature for all the Ni-W-B samples. There were two reasons for superior corrosion resistance of Ni-W-B alloy films; one is preferential dissolution of Ni and formation of W-rich film on the surface, which inhibited further corrosion. During the corrosion process tungsten preferentially migrates toward the surface and forms oxides; other reasons are water molecules which are absorbed on the electrode surface and the formation of Ni(OH)₂ passive films, according to the following different mechanisms involving chemical and electrochemical steps [30, 31]:



The insoluble Ni(OH)₂ covers the surface of the corroded samples and creates the passivation region (approximately from +0.35 V to +1.55 V) where the current density is almost independent of the potential. With an increase of potential up to approximately +1.55 V, the anodic current density dramatically increases with the increase of potential, indicating the breakdown of the surface Ni(OH)₂ passive film and the occurrence of pitting corrosion in Ni-W-B coatings.

3.7. EIS measurements at different anodic potentials

Equivalent circuits and the influence of the different anodic potentials on the impedance pattern of Ni-38.94 wt. %W-1.86 wt. %B alloy coatings in 1 N sulfuric acid solution are presented in Figure 10.

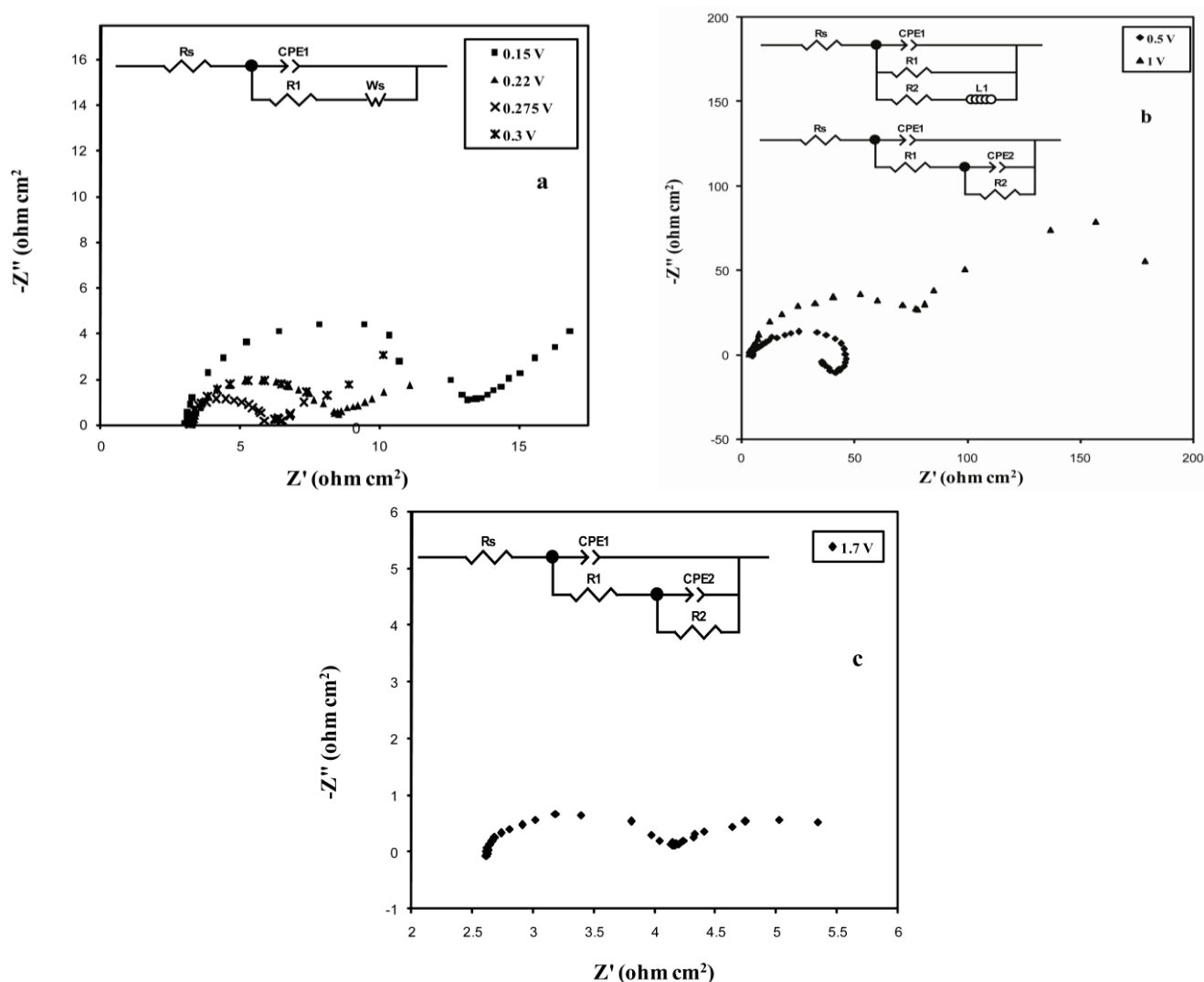


Figure 10. Equivalent circuits and Nyquist's plots of Ni-38.94 wt. %W-1.86 wt. %B alloy deposited from solution with 0.5 g L⁻¹ BD concentration in 1 N H₂SO₄ at different anodic potentials

The EIS measurements were carried out sequentially starting with freshly Ni-W-B samples and polarizing it at increasingly anodic potentials. The equivalent circuit model and the Nyquist diagrams of Ni-38.94 wt. %W-1.86 wt. %B alloy coatings in the potential range 0.15-0.3 V are shown in Figure 10a (active region). In this model, R_s , R_1 , CPE_1 and W are the solution resistance, the charge transfer resistance, constant phase element and Warburg diffusion impedance, respectively.

In the potential range 0.15-0.275 V, one can observe a poorly defined high-frequency capacitive loop, followed by a Warburg type behavior linked to the diffusive electro-kinetic control. This kind of behavior can be related to mass-transport controlled dissolution of the Ni-W-B alloy. In this region, with increasing of potential, the values of R_1 of samples tend to decrease, indicating an easier diffusion of species to the electrode surface and a faster electrochemical reaction process, as the least of the charge transfer resistance can be seen in anodic nose (0.275 V). In potential of 0.3 V, that is required potential for forming of the passive film, corrosion resistance of coating increased somewhat.

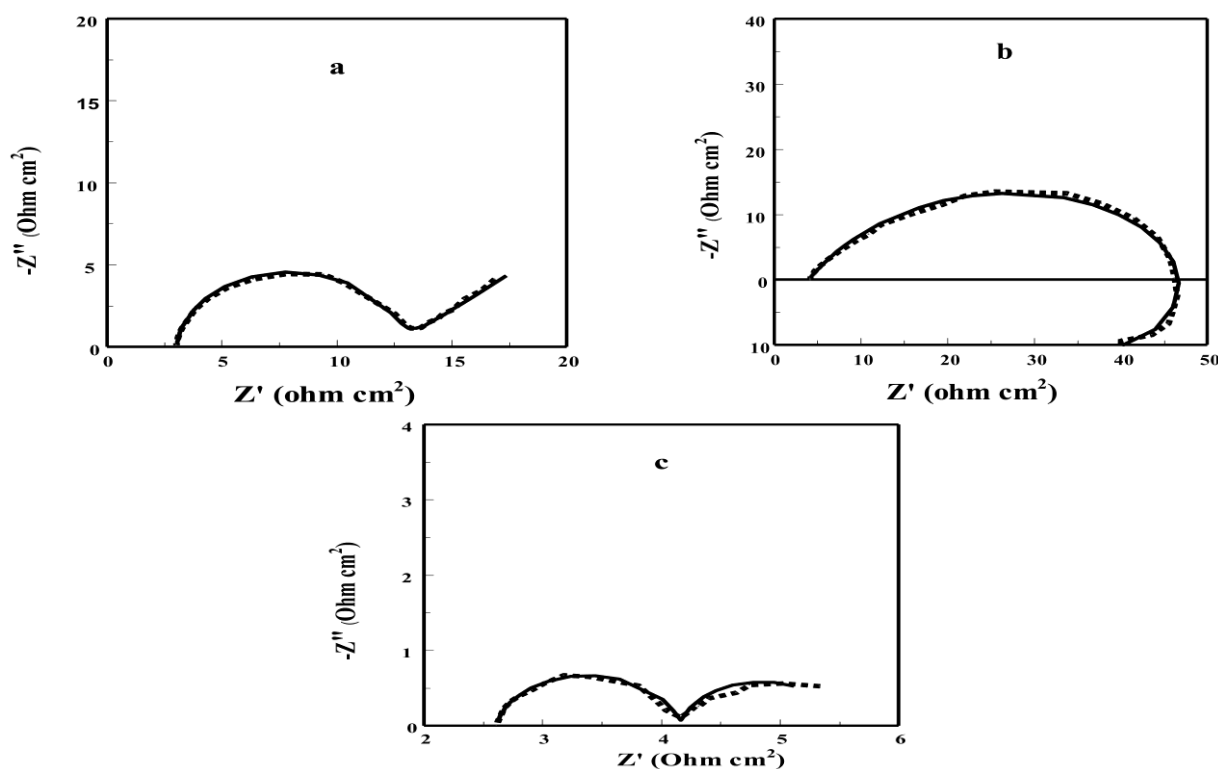


Figure 11. Nyquist diagrams (dotts) and the fitted curves (solid lines) of Ni-38.94 wt. %W-1.86 wt. %B alloy deposited at solution with 0.5 g L^{-1} BD concentration in $1 \text{ N H}_2\text{SO}_4$ at potentials (a) 0.15 V (b) 0.5 V and (c) 1.7 V vs. SCE.

Generally, corrosion rate is affected by the dissolution of Ni together with the inter-diffusion of Ni^{2+} and OH^- ions to the electrode surface. In potential of 0.5 V, the complex plane plot presented only one capacitive loop and one inductive loop at low frequencies (Figure 10(b)); the capacitive loop is associated with the double layer capacity and the inductive loop can be associated with the

adsorption/desorption process. In corresponding equivalent circuit, R_2 and L_1 are the resistance and inductance related to the adsorption/desorption process, respectively. In potential of 1 V, there are two time constants in the impedance spectrum (Figure 10b).

Table 4. Fitting results of the impedance spectra of Ni-38.94 wt. %W-1.86 wt. %B alloy at different anodic potentials in 1 N H_2SO_4 solution.

Element	0.15 V	0.22 V	0.275 V	0.3 V	0.5 V	1 V	1.7 V
R_s ($\Omega\text{ cm}^2$)	3.044	3.29	3.043	3.342	4.005	4.193	2.612
CPE_1 ($F\text{ cm}^2$)	0.0001157	0.00012172	0.000062907	0.000055659	0.001279	0.00039335	0.0016316
R_1 ($\Omega\text{ cm}^2$)	9.555	4.342	0.0016149	0.66836	48	83.02	1.546
CPE_2 ($F\text{ cm}^2$)	-	-	-	-	-	0.0097989	3.886
R_2 ($\Omega\text{ cm}^2$)	-	-	-	-	56	184.9	1.385
L_1 ($H\text{ cm}^2$)	-	-	-	-	57	-	-
W_1 ($\Omega\text{ s}^{-1/2}$)	51.4	42.93	3.675	466.7	-	-	-
Error (%)	0.037	0.044	0.04	2.9	1.67	2.73	0.1

In this potential, an equivalent circuit consisting of two RC circuits shown was proposed. Circuit R_2CPE_2 describes the electrode Faraday process (nickel oxidation) and corresponds to low-frequency impedance while circuit R_1CPE_1 represents the presence of a surface film and corresponds to high-frequency impedance. Generally, in potentials of 0.5 V and 1 V (passive region), because of formation of the WO_3 , NiO and $Ni(OH)_2$ films, corrosion resistance of coating increased very much (Figure 10b).

The Nyquist plot at potential of 1.7 V, corresponding to trans-passive region is shown in Figure 10c. In this potential, an equivalent circuit consisting of two RC circuits is also proposed. In this region, due to break down of passive film, both the charge transfer resistance and the resistance of the film drop drastically. Generally, decrease in the resistance values during of the active region was ascribed to the dissolution of Ni, while the increasing resistance was attributed to the presence of corrosion products on the surface, which improved the barrier properties. This feature is typical of a surface containing corrosion products that act as a barrier against corrosion.

The Figure 11 shows that the fitting data have good correlation with experimental impedance results. The corresponding data for each element are listed in Table 4. The goodness of the fit can be judged by the estimated relative errors as presented in Table 4 and by the fitting lines in Figure 11.

4. CONCLUSIONS

Based on the results obtained in the present investigation on electrodeposited nanocrystalline Ni-W-B alloys in the presence and absence of BD the following conclusions have been drawn: The incorporation of BD into the plating bath resulted in inhibition of crystal growth, reduction of surface

roughness, increase in surface brightness and sharp reduction of grain size. The microhardness of as-plated Ni-W-B coatings reaches 875 HV that is comparable to the hardness of traditional electrodeposited chromium. Based on the results and discussion for the corrosion potential, corrosion current and corrosion resistance from the electrochemical polarization methods and the corrosion resistance from the EIS technique, the Ni-38.94 wt. %W-1.86 wt. %B alloys deposited at solution with 0.5 g L^{-1} BD concentration are concluded to be the best corrosion resistant coatings compared to those of the alloys deposited at solution without BD. The superior corrosion resistance of Ni-W-B alloy films was due to preferential dissolution of nickel and formation of tungsten rich film or $\text{Ni}(\text{OH})_2$ passive films on the surface. All the Ni-W-B samples exhibited active-passive-transpassive polarization behavior due to the reasons mentioned above. The shift of OCP toward more the noble potential with decreasing grain size has been related to modification in cathodic reaction (hydrogen reduction) processes. The mechanism of onset of passivity and passivation itself is similar in nature for all the Ni-W-B samples.

ACKNOWLEDGEMENT

The authors would like to acknowledge the financial support of Iranian Nanotechnology Society and the Office of Vice Chancellor in Charge of Research of University of Tabriz.

References

1. J.H. Lindsay, *Plat. Surf. Finish.* 82 (1995) 19.
2. P.C. Wynn, C.V. Bishop, *Trans. IMF.* 79 (2001) 27.
3. J. N. Balaraju and K. S. Rajam, *Int. J. Electrochem. Sci.*, 2 (2007) 747 – 761. [20]
4. E. Lassner, W.D. Schubert, *Tungsten - Properties, Chemistry, Technology of the Element, Alloys, and Chemical Compounds*, Springer, 1999.
5. E. Beltowska-Lehman, *Phys. Stat. Sol.* 5 (2008) 3514.
6. E.J. Podlaha, D. Landolt, *J. Electrochem. Soc.* 143 (1996) 885.
7. E.J. Podlaha, D. Landolt, *J. Electrochem. Soc.* 144 (1997) 1672.
8. M. Donten, H. Cesiulis, Z. Stojek, *Electrochim. Acta.* 45 (2000) 3389.
9. A. Brenner, *Electrodeposition of Alloys 2*, Academic Press Inc, New York, 1963.
10. T. Yamasaki, P. SchloBmacher, K. Ehrlich, Y. Ogino, *Nanostruct. Mater.* 10 (1998) 375.
11. M. Donten, T. Gromulski, Z. Stojek, *J. Alloys and Comp.* 279 (1998) 272.
12. [R.M. Krishnam, Kennedy C. Joseph, Jayakrishnam Sobha, S. Sriveeraraghavan, S.R. Natarajam, *Met. Finish.* 7 (1995) 33.
13. G.E. Shahin, *Plat. Surf. Finish.* 85 (1998) 8.
14. H. Capel, P.H. Shipway, S.J. Harris, *Wear.* 255 (2003) 917.
15. M. Jayalakshmi, Woo-Young Kim, Kwang-Deog Jung, Oh-Shim Joo, *Int. J. Electrochem. Sci.*, 3 (2008) 356 – 408
16. E.W. Brooman, *Met. Finish.* 99 (2004) 42.
17. S. Latif, M. Mehmood, J. Ahmad, M. Aslam, M. Ahmed, Z.D. Zhang, *Appl. Surf. Sci.*, 256 (2010) 3098.
18. M.G. Hosseini, M. Abdolmaleki, S.A. Seyed Sadjadi, *Protection of Metals and Physical Chemistry of Surfaces.* 45 (2009) 757.
19. M.G. Hosseini, M. Abdolmaleki, S.A. Seyed Sadjadi, M. Raghibi Boroujeni, M.R. Arshadi, H. Khoshvaght, *Surf. Eng.* 25 (2009) 382.

20. M. G. Hosseini, M. R. Arshadi, *Int. J. Electrochem. Sci.*, 4 (2009) 1339 – 1350.
21. .R. Yazdzad, T. Shahrabi, M.G. Hosseini, *Mat. Chem. Phy* 109 (2008) 199.
22. T. Shahrabi, A.R. Yazdzad, M.G. Hosseini, *J. Mat. Sci. Tech.* 24 (2008) 427.
23. N. Eliaz, . TM. Sridhar, E. Gileadi, *Electrochim. Acta.* 50 (2005) 2893.
24. B.D. Cullity, *Elements of X-Ray Diffraction*, 2nd ed, Addison-Wesley, Reading, 1978, p. 281.
25. T. Omi, H.L. Glass, H. Yamamoto, *J. Electrochem. Soc.* 123 (1976) 341.
26. T. Omi, H. Yamamoto, H.L. Glass, *J. Electrochem. Soc.* 119 (1972) 168.
27. W.S. Tait, *An Introduction to Electrochemical Corrosion Testing for Practicing Engineers and Scientists*, Pair O Docs Publications, Racine, WI, 1994, pp. 79 and 95.
28. I.D. Raistrick, J.R. Macdonald (Ed.), D.R. Franceschetti, *Impedance Spectroscopy*, Wiley, New York, 1987, p. 27.
29. Gamry Instruments, Warminster, PA. Application Notes, in “The Basics, Electrochemical Impedance Spectroscopy: A Primer”, (Gamry Instruments, Warminster PA, 2000).
30. W.A. Badawy, K.M. Ismail, A.M. Fathi, *Electrochim. Acta.* 50 (2005) 3603.
31. W.A. Badawy, F.M. Al-Kharafi, J.R. Al-Ajmi, *J. Appl. Electrochem.* 30 (2000) 693.